

## Research Article

# Thermal Analysis of Building Roofs with Latent Heat Storage for Reduction in Energy Consumption and CO<sub>2</sub> Emissions: An Experimental and Numerical Research

Erdem Cuce <sup>1,2,3</sup>, Saboor Shaik <sup>4</sup>, Abin Roy <sup>4</sup>, Chelliah Arumugam <sup>5</sup>, Asif Afzal <sup>6,7</sup>, Pinar Mert Cuce <sup>1,8</sup>, Aritra Ghosh <sup>9</sup>, Tabish Alam <sup>10,11</sup> and Sharmas Vali Shaik <sup>12</sup>

<sup>1</sup>Low/Zero Carbon Energy Technologies Laboratory, Faculty of Engineering and Architecture, Recep Tayyip Erdogan University, Zihni Derin Campus, Rize 53100, Türkiye

<sup>2</sup>Department of Mechanical Engineering, Faculty of Engineering and Architecture, Recep Tayyip Erdogan University, Zihni Derin Campus, Rize 53100, Türkiye

<sup>3</sup>School of Engineering and the Built Environment, Birmingham City University, Birmingham B4 7XG, UK

<sup>4</sup>School of Mechanical Engineering, Vellore Institute of Technology Vellore, Vellore 632014, Tamil Nadu, India

<sup>5</sup>Department of Mechanical Engineering, SRM Institute of Science and Technology, Ramapuram Campus, Chennai 600089, Tamil Nadu, India

<sup>6</sup>Department of Mechanical Engineering, P. A. College of Engineering (Affiliated to Visvesvaraya Technological University Belgavi), Mangaluru 574153, India

<sup>7</sup>Department of Computer Science and Engineering, University Centre for Research & Development, Chandigarh University, Gharuan, Mohali, Punjab, India

<sup>8</sup>Department of Architecture, Faculty of Engineering and Architecture, Recep Tayyip Erdogan University, Zihni Derin Campus, Rize 53100, Türkiye

<sup>9</sup>Faculty of Environment, Science and Economy (ESE), Renewable Energy, Electric and Electronic Engineering, University of Exeter, Penryn TR10 9FE, UK

<sup>10</sup>CSIR—Central Building Research Institute, Roorkee 247667, Uttarakhand, India

<sup>11</sup>Academic of Scientific and Innovative Research (AcSIR), Ghaziabad 201002, Uttar Pradesh, India

<sup>12</sup>Department of Mechanical Engineering, Srinivasa Ramanujan Institute of Technology (Autonomous), Anantapur 515701, Andhra Pradesh, India

Correspondence should be addressed to Erdem Cuce; [erdem.cuce@erdogan.edu.tr](mailto:erdem.cuce@erdogan.edu.tr) and Saboor Shaik; [saboor.nitk@gmail.com](mailto:saboor.nitk@gmail.com)

Received 27 January 2023; Revised 20 July 2023; Accepted 12 October 2023; Published 19 February 2024

Academic Editor: Robert Černý

Copyright © 2024 Erdem Cuce et al. This is an open access article distributed under the Creative Commons Attribution License, which permits unrestricted use, distribution, and reproduction in any medium, provided the original work is properly cited.

In green energy buildings, air conditioning charges can be lowered through careful planning of the building's envelope. This article investigates several strategically designed phase change material (PCM) roof envelopes for savings on air conditioning prices, CO<sub>2</sub> emission abatement, and payback timeframes in hot–arid and warm-temperate climates, taking into account unsteady heat transfer characteristics, cooling, and heating degree–hours. This is accomplished by using six different PCMs—RCC (reinforced cement concrete) roof envelope cases (RCC roof with PCM layer on the outer side, RCC roof with PCM layer on the center (middle), RCC roof with PCM layer on the inside, RCC roof with PCM layers placed on the outside and center, RCC roof with PCM layers placed on the center and inside, and RCC roof with PCM layers placed on the outer side and inside) with three PCMs (FS29 (form stable mixture), HS29 (hydrated salt), and OM29 (organic mixture)). PCM thermophysical characteristics are experimentally measured. The analytical results are experimentally validated. In hot–arid and warm-temperate regions, the layer of PCM installed on the outside of the RCC with HS29 saved the most on air conditioning expenses, at 6.29 and 6.61 \$/m<sup>2</sup>, respectively. They also reported the greatest carbon mitigation of 300.55 kg of CO<sub>2</sub>/year and 281.58 kg of CO<sub>2</sub>/year with the faster payback periods. PCM roof envelopes are the most energy-efficient option for green buildings.

## 1. Introduction

There has been a noticeable rise in energy consumption in both domestic and industrial buildings in recent years. This increase in energy usage is primarily driven by factors such as global warming, the need for thermal comfort, and the growing energy demand associated with economic development, population growth, and rapid urbanization, especially in developing countries. Buildings are major consumers of energy, particularly for functions like air conditioning and lighting. Cooling systems account for a substantial portion of energy consumption in buildings, especially in regions with hot climates.

Energy shortage and environmental pollution are two worldwide concerns that must be addressed as soon as possible. Energy conservation is the critical importance to the growth of the global economy and society [1]. Buildings account for approximately 40% of global energy consumption. Within the building sector, residential buildings alone contribute to 75% of energy usage and one-third of greenhouse gas emissions [2]. In India, buildings consume around 35% of the country's total energy, and this consumption is growing at a rate of 8% annually [3]. Rapid urbanization and population growth contribute to an annual increase of 1.8% in building construction. These trends further amplify the energy demand and environmental challenges associated with the building sector [4]. Northern India experiences extreme variations in weather conditions, with both hot summers and cold winters. This necessitates the use of heating, ventilation, and air conditioning systems, which consume a substantial amount of energy, contributing to the overall energy consumption in buildings [5].

The heat storage characteristics of different parts of a building's envelope, such as walls, roofs, and windows, are closely linked to their exposure to solar radiation and can vary depending on the season of the year [6]. Several new building standards have emerged, including the passive house standard, which is a stringent energy-use standard observed on a highly insulated and tightly sealed building envelope [7]. PCMs have gained popularity in building-related applications due to their large energy storage and stability capabilities [8]. The PCMs usage in building components and envelopes shifts peak energy loads, dampens incoming solar radiation, and improves thermal comfort [9–12]. The PCM-integrated building façade conserves both space and energy by removing the requirement for HVAC systems auxiliary equipment like compressors, refrigerant storage containers, and condensers [13]. PCM is the most often employed latent heat storage material since they are capable of transitioning from a solid to a liquid form and back again [14]. There is a variety of options available to incorporate PCM in buildings. It can be added to the wall, floor, or ceiling [15].

When the temperature rises over a certain threshold, the chemical components in the PCM's solid start to absorb heat and break apart, resulting in an endothermic reaction that causes the substance to transition from solid to liquid [16]. Some studies have investigated the use of organic PCMs like paraffin and fatty acids for low thermal energy storage

purposes because of desirable qualities, including excellent heat storage density, chemical stability, and cheap cost [17]. Differential scanning calorimetry (DSC) was used to determine the PCM's thermal properties, like melting and freezing temperatures and latent heat capacity [18]. Organic PCMs are distinguished by noncorrosive characteristics and melting points that are close to one another [19]. The method of embedding PCMs in encapsulation material greater than 1 mm in size is known as macroencapsulation, and it may be used in any building enclosure type and size [4].

The capacity of various macroencapsulations of PCM and enclosing substances to give excellent indoor thermal comfort in building applications was explored [20]. The PCM design integrated building needs a thorough investigation of various factors, including operational climatic conditions, materials employed, and structural geometric qualities [21]. It shows a novel construction consisting of an encapsulated PCM that was placed in the hollow core plate. This technology has the ability to increase the utilization of energy storage cooling factor with the usage of night ventilation [22].

A numerical and experimental analyses were done in Istanbul to examine the integration of PCMs into the roof and simulation results revealed that 2 cm PCM layer thickness was adequate for flat roof applications [23]. The thermal efficiency of a PCM-layered roof in Chennai was investigated, and it was noted that double-layer PCM boosted thermal comfort in the building [24]. Five distinct PCMs were tested in terracotta bricks under hot-dry climatic conditions in India, and it was discovered that there is a reduction in the cost of conditioning by about \$74.70 per year while incorporating OM32 PCM [25]. To examine the thermal mass effect on the room temperature, a glass building model containing macropacked PCM was included into the structure [26]. Empirical research was carried out in Guangzhou to assess the endurance of a PCM that was installed on the outside of the roof. The thermal insulating capability of the roof with phase change material was found to be equivalent to that of the green roof and somewhat superior to that of the EPS roof, according to the test results [27]. Under hot-dry climatic conditions in India, the experimental investigation was conducted in the building prototype in which the roof was built with the filler slab stuffed with form stable PCM. The researchers concluded that there was an indoor temperature reduction from 8 to 10°C compared to the conventional reinforced concrete slab [28].

The thermoeconomic performance of PCM stuffed buildings may be assessed using the technique of heating and cooling degree days, which is among the simplest strategies for determining the building's thermoeconomic performance [29]. Using Energy Plus, the effect of PCM on the energy consumption of buildings was simulated for a full year in five Chinese cities around the nation. The findings have shown that buildings equipped with PCMs may save a large amount of energy [30]. PCM was thermally analyzed theoretically and experimentally in a vertical cylinder hole formed into a concrete roof. It lowers the inside building's heat flow by 17.26% [31].

TABLE 1: M15 mixed proportion for RCC slab.

S. No.	Roof material	Required quantity (kg/m <sup>3</sup> )
1.	Cement	317
2.	Fine aggregate	713
3.	Coarse aggregate	1,364
4.	Water	190
5.	MS steel	80

The aforementioned literature survey provides relatively scant knowledge on PCM roof envelopes for cost savings and CO<sub>2</sub> reductions in buildings. Recent studies have shown that the type, thickness, and position of PCM have a significant impact on the thermal performance of building systems. Integrating PCMs into roofs is a great approach to increasing the thermal mass of the intended part and, thus, reducing daily temperature changes. To determine the best location of PCM in RCC roofs for the optimum air conditioning cost savings and carbon emission mitigations, six unique configurations for inserting PCM in RCC roofs are presented (Section 2.1) for buildings in hot–arid and warm-temperate climates. Three PCMs (FS29, HS29, and OM29) were studied experimentally for their thermophysical properties (Section 2.2). The mathematical model simulations (Section 2.3) are validated by the experimental findings. Methodology for thermal performance, energy cost savings, and CO<sub>2</sub> reductions of PCM integrated roofs are presented in detail (Section 2.4). The results (Section 3) are significant for engineers and architects adopting PCM roof envelopes for energy-efficient buildings.

## 2. Materials and Methods

**2.1. Materials.** The roof is composed of reinforced cement concrete (RCC) having grade M 15 of IS 10262:2019 [32]. The components used for the preparation of the RCC roof are cement, coarse aggregate, fine aggregate, steel bars, binding wire, and water. Shuttering materials are provided at the construction time of the RCC roof. For finishing, plaster is often applied to both the inner and outer surfaces of the roofs. Table 1 represents the required quantity for RCC slab.

In this work, the macroencapsulated PCM's energy performance in various locations on the roof structure was compared. FS29, HS29, and OM29 have a melting point of 29°C. PCMs having this melting point are suitable for the passive cooling of buildings in the warm climatic conditions in India. OM29 since organic PCM has consistent physical and chemical properties, a large latent heat capacity, and the right phase transition temperature, is noncorrosive, and melts uniformly. Form-stable PCM (FS29) is the combination of organic and inorganic mixtures. Also, HS29 since the fundamental benefit of inorganic PCMs (metals, salt solutions, and salt hydrates) over organic PCMs is their higher heat of fusion per unit mass, lower cost, and high thermal conductivity (TC) [4]. Polyethylene glycol, in conjunction with paraffin, fatty acids, and their mixes, is form stable [33]. The different PCMs investigated are FS29 (form stable mixture),

HS29 (hydrated salt), and OM29 (organic mixture) to realize the thermoeconomic analysis. The macroencapsulated PCMs are placed; case (a) and (b) on the external side of the RCC, case (c) and (d) in between the RCC, case (e) and (f) on the inside of the RCC, case (g) and (h) outside and middle of the RCC, case (i) and (j) in middle and inside of the RCC, and case (k) and (l) PCM layer is placed outside and inside of the RCC. Table 2 represents the various configurations of the RCC slab taken for the study, while Figure 1 provides a visual illustration of the RCC roof filled with PCMs.

**2.2. Experimental Methodology.** Figure 2 shows an experimental arrangement for measuring the thermophysical characteristics of RCC and PCMs. The viscometer contains cooling and heating units that raise and lower the temperature of PCMs to determine the TC value of solid and liquid stages. Externally, surrounding the cup, PCMs were surrounded by water at the required temperature. Using the digital reading display, the proper temperature has been maintained.

The TC of PCMs was measured in accordance with the ASTM standard by the KD2 thermal property analyzer (KD2 Probe) [34]. The probe consists of two pins: the first one is an electric pulse heating source and the second one serves as a receiver. Pins have the dimensions of 1.3 mm in diameter and 3 cm in length and are spaced 6 mm apart. The resulting temperatures in the time domain define the TC of the PCMs in both phases within ±10% accuracy. The volumetric-specific heat can also be calculated with ±10% accuracy.

The density of PCM was measured by the specific gravity bottle method with an accuracy of ±1%. The measured volume of liquid PCM was taken in the bottle, and the bottle filled with a known volume of liquid PCM was weighed on the weighing machine. The difference between the mass of the bottle and the mass of the bottle filled with PCM gave the mass of liquid PCM. The density was measured by the mass and volume of liquid PCM. Specific gravity was used to determine the PCM's liquid volume, density, and weight [35]. The specific heat and TC values of the plaster, the concrete roof, also investigated PCMs (both solid and liquid states) were calculated (uncertainty values:  $k = \pm 0.00234$  W/(m K),  $C_p = \pm 3$  J/(kg K),  $\rho = \pm 2$  kg/m<sup>3</sup>) [36]. The DSC method was used to determine the phase transition temperatures and the latent heats of PCMs are represented in Table 3 [18]. The PerkinElmer equipment has a temperature between −180 and −450°C with the ±2% accuracy. The temperature and heat flow were calibrated with the usage of 10 mg of zinc and indium.

**2.3. Analytical Methodology.** Mathematical model simulations use the admittance technique to compute cyclic transmittance which takes into account properties ( $k$ ,  $C_p$ , and  $\rho$ ). The method is presented below [37].

$$\frac{\partial^2 \theta}{\partial y^2} = \frac{\rho C_p}{\delta} \frac{\partial \theta}{\partial t}. \quad (1)$$

The expression equation provides the solution to the Fourier problem for the aforementioned Equation (2):

TABLE 2: RCC roof configuration and cross-section thickness.

S. No.	Roof configuration	Cross-section thickness of the roof (m)
1	Traditional roof	$0.015P + 0.17RCC + 0.015P$
2	R-1 (outer)	$0.015P + 0.02PCM + 0.15RCC + 0.015P$
3	R-2 (middle)	$0.015P + 0.075RCC + 0.02PCM + 0.075RCC + 0.015P$
4	R-3 (inner)	$0.015P + 0.15RCC + 0.02PCM + 0.015P$
5	R-4 (outer-middle)	$0.015P + 0.01PCM + 0.070RCC + 0.01PCM + 0.080RCC + 0.015P$
6	R-5 (middle-inner)	$0.015P + 0.080RCC + 0.01PCM + 0.070RCC + 0.01PCM + 0.015P$
7	R-6 (outer-inner)	$0.015P + 0.01PCM + 0.15RCC + 0.01PCM + 0.015P$

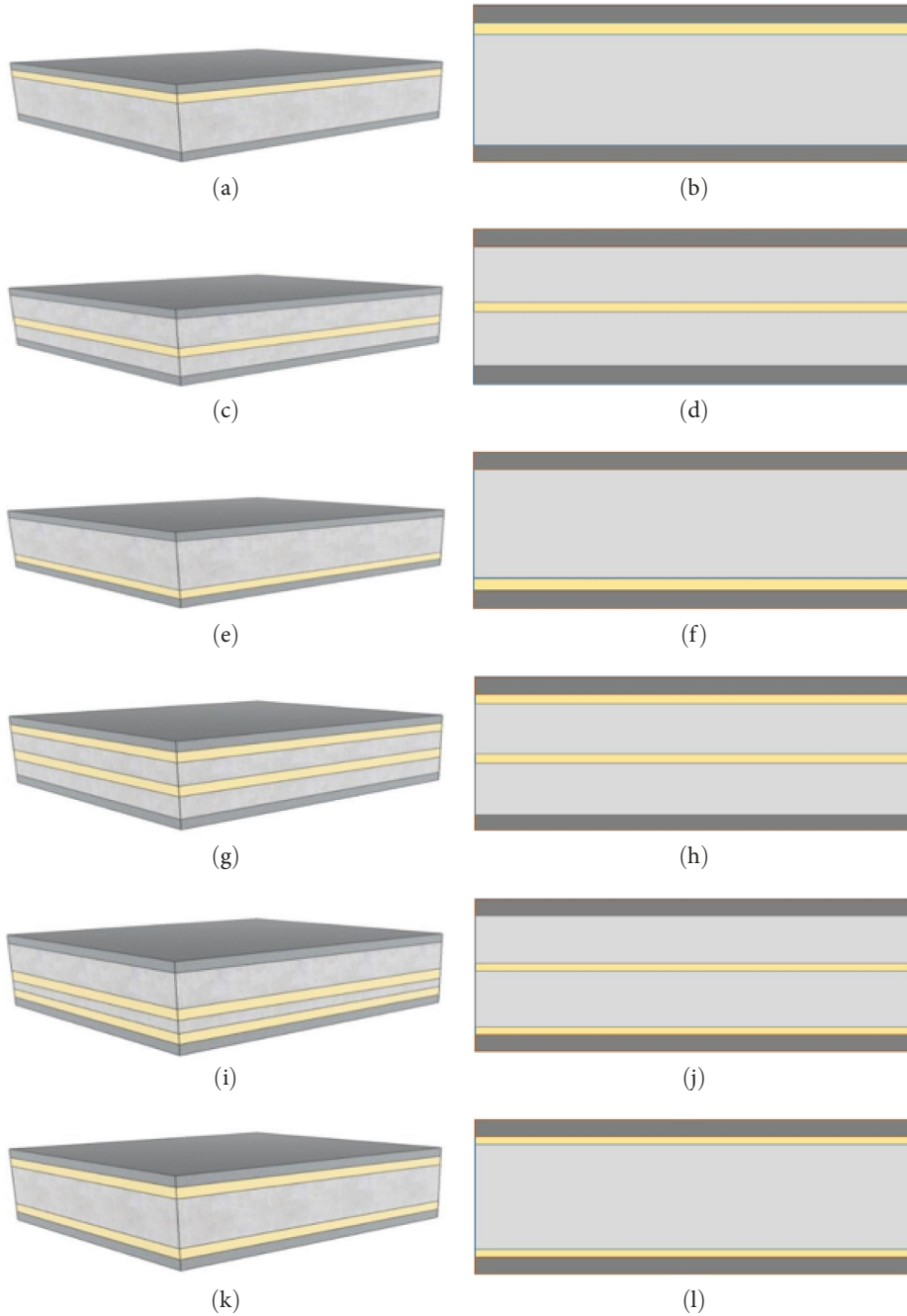


FIGURE 1: Diagrammatic representation of the RCC roof stuffed with PCMs. RCC roof with PCM pleats; on the outer side (R-1) (a) and (b), on the center (R-2) (c) and (d), on the inside (R-3) (e) and (f), in the center and outside (R-4) (g) and (h), in the center and inside (R-5) (i) and (j), and placed on the inside and outer side (R-6) (k) and (l).

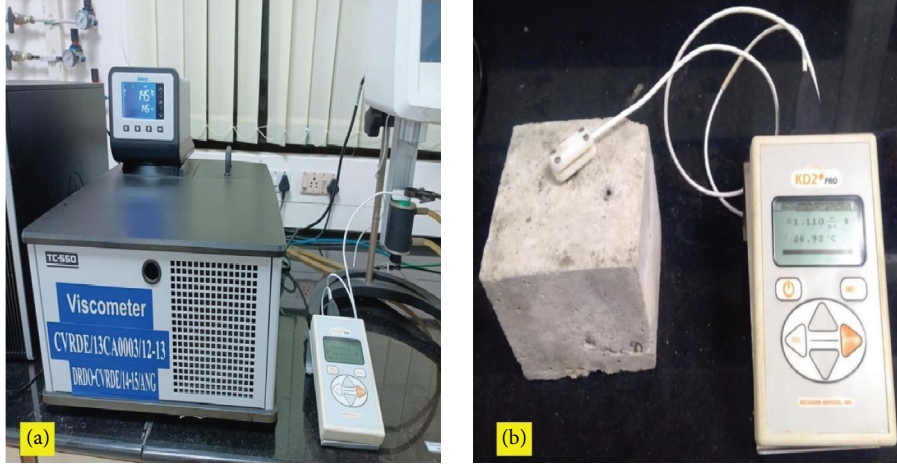


FIGURE 2: (a) PCM thermal parameters measured using KD2 Pro and viscometer; (b) KD2 Pro determining the thermal characteristics of RCC roof.

TABLE 3: Roof envelope materials thermophysical properties.

PCM	Latent heat (H) J/kg	Phase transition range (°C)	PCM temperature (solid phase) (°C)	$k$ (W/(m K))		PCM temperature (liquid phase) (°C)	$C_p$ (J/(kg·K))		$\rho$ (kg/m <sup>3</sup> )	
				Solid	Liquid		Solid	Liquid	Solid	Liquid
FS29	160	22–32	22	0.55 ± 0.002	0.45 ± 0.001	29	2,700 ± 3	2,100 ± 2	1,040 ± 3	952 ± 4
HS29	190	24–34	24	0.48 ± 0.004	0.38 ± 0.004	29	1,510 ± 2	2,320 ± 3	1,681 ± 5	1,530 ± 3
OM29	194	24–33	24	0.29 ± 0.003	0.17 ± 0.004	29	2,330 ± 3	2,720 ± 1	976 ± 4	880 ± 5
OM30	230	23–32	14.5	0.16 ± 0.002	0.15 ± 0.003	32	2,040 ± 4	2,780 ± 3	950 ± 6	878 ± 6
Plaster	–	–	–	0.72 ± 0.003	–	–	840 ± 1	–	1,760 ± 5	–
RCC	–	–	–	1.58 ± 0.002	–	–	1,100 ± 2	–	2,280 ± 2	–
Galvanized iron casing	–	–	–	61.06 ± 0.005	–	–	500 ± 0.04	–	7,520 ± 2	–

$$\theta(y, t) = [H_{r1} \sinh \sinh(b + jb) + T_{r1} \cosh \cosh(b + jb)] \exp\left(\frac{j2\pi t}{p}\right), \quad (2)$$

where  $b = \sqrt{\rho c_p y^2 / kp}$ ,  $\theta$  represents the temperature,  $t$  stands for the cyclic thickness,  $y$  stands for the diameter of the

structural materials,  $p$  indicates the cyclic period,  $C_p$  stands for the specific heat,  $\delta$  represents the TC,  $\rho$  denotes the density,  $H_{r1}$  indicates the heat flow from the external of the roof,  $T_{r1}$  denotes thermal resistance, whereas  $j$  is an imaginary variable.

In the transmission matrix, the above equations should be altered as shown in Equation (3):

$$[\theta_{in} \ q_{in}] = \left[ \cosh \cosh(b + jb) \left( \frac{\sinh \sinh(b + jb)}{d} \right) \right] d (\sinh \sinh(t + jb) \cosh \cosh(t + jb)) [\theta_{ou} \ q_{ou}], \quad (3)$$

where  $d$  is the characteristic admittance of the concrete surface,  $(d) = \sqrt{j2\pi k \rho y^2 C_p / p}$ ,  $\theta_{in/ou}$  is the periodic temperature of the inner and outer, and  $q_{in/ou}$  is the cyclic heat flow between inside and outside.

The following equation describes the transmission matrix for normal and PCM roof envelops:

$$[\theta_{in} \ q_{in}] = [1 - h_{in}^{-1} 0 1] [d_1 d_2 d_3 d_1] [e_1 e_2 e_3 e_1] \cdot [1 - h_{ou}^{-1} 0 1] [\theta_{ou} \ q_{ou}]. \quad (4)$$

In Equation (4), the indications  $d$  and  $e$  stand for distinct construction materials. For the roof case, the outside and inner heat transfer coefficients ( $(h_{ou})$  and  $(h_{in})$ ) of roofing materials are 25 and 10 W/m<sup>2</sup>K, respectively.

$$[\theta_{in} \ q_{in}] = [V_1 \ V_2 \ V_3 \ V_1] [\theta_{ou} \ q_{ou}]. \quad (5)$$

Increasing or decreasing heat absorption on the inside of a roof design due to variations in outside temperature is represented by the cyclic transmittance ( $u_{cy}$ ) of a roof layout.

TABLE 4: Thermophysical properties of roof materials for verification MATLAB code.

Thermophysical properties	Values
Density ( $\rho$ )	1,940 kg/m <sup>3</sup>
Specific heat ( $C_p$ )	840 J/kgK
Thermal conductivity ( $k$ )	0.83 W/mK

The lower amount of unsteady transmittance in the normal and PCM-included roof arrangements suggests a minimal heat transfer into the interior of the structure, which can be calculated using Equation (6) [38].

$$u_{cy} = \left| -\frac{1}{V_2} \right|. \quad (6)$$

The cycle transmittance of construction materials has been calculated using a MATLAB program that has been verified in accordance with the CIBSE standard. The thermophysical attributes of roof materials are depicted in Table 4. According to the results, the cyclic transmittance value of the roof material was defined to be 2.19 W/m<sup>2</sup>K, which is identical to the value of 2.19 W/m<sup>2</sup>K found in the CIBSE roof standard. There is even less than 1% (0.7%) variance between the MATLAB program and the CIBSE reference, which means that MATLAB code is regarded as trustworthy for usage with other kinds of building materials too [39–41].

**2.3.1. Thermoeconomic Analysis.** The annual energy consumption of buildings was determined by the number of degree-hours needed for cooling and heating. Specifically, the thermoeconomic performance of PCM roof envelopes was evaluated in two locations in India: (21.20°N 72.83°E) Surat (hot-arid) and (28.57°N 75.12°E) New Delhi (warm-temperate). ASHRAE meteorological parameters were used to calculate heating and cooling degree-hours for Surat and New Delhi, India, considering 18 and 26.7°C as the corresponding reference temperatures. As shown in Figure 3, the annual cooling degree-hours in Surat and New Delhi are 17,891 and 25,343°C hr, respectively, whereas the annual heating degree-hours are 0 and 6,864°C hr, respectively [42].

The latent heat release and absorption of the PCMs such as FS29, HS29, and OM29 have been computed using Equations (7)–(13) [43].

$$L_{fig} = \omega_1 H, \quad (7)$$

where  $L_{fig}$  represents PCM's latent heat utilization,  $H$  denotes latent heat values of PCM's latent heat, and  $\omega_1$  indicates a liquid fraction.

$$\omega_1 = 1, \text{ if } \theta_a > \theta_1, \quad (8)$$

where  $\theta_a$  indicates mean ambient temperature and  $\theta_1$  indicates melting PCM temperature.

The liquid fraction is treated as being one when the average ambient temperature ( $\theta_a$ ) is higher than PCM's

melting temperature ( $\theta_1$ ).

$$\omega_1 = \frac{\theta - \theta_s}{\theta_1 - \theta_s}, \text{ if } \theta_1 < \theta_a > \theta_s. \quad (9)$$

When the typical ambient temperature is between the PCM's melting and freezing temperatures, the PCM is in the sticky zone. Throughout the sticky zone, the liquid percentage varies between 0 and 1.

$$\omega_1 = 0, \text{ if } \theta_a < \theta_s. \quad (10)$$

It is considered that the liquid fraction equals zero since the mean temperature of the ambient air ( $\theta_a$ ) is lower than the temperature at which the PCM ( $\theta_s$ ) freezes.

$$\omega_s = 1, \text{ if } \theta_a < \theta_s. \quad (11)$$

As long as the normal surrounding temperature ( $\theta_a$ ) is lower than the freezing point of the PCM ( $\theta_s$ ), the solid fraction is 1.

$$\omega_s = 1 - \omega_1, \text{ if } \theta_L < \theta_a > \theta_s. \quad (12)$$

During the sticky zone, the solid fraction fluctuates from 0 to 1.

$$\omega_s = 0, \text{ if } \theta_a > \theta_1. \quad (13)$$

The solid fraction is zero, as long as the mean ambient temperature ( $\theta_a$ ) is more than PCM's melting temperature ( $\theta_s$ ) [44].

In this study, PCM's phase change temperature is based on the mean temperature of the atmosphere. Figures 4(a) and 4(b) displays the temperature readings for Surat and New Delhi [45]. Monthly minimum, average, and maximum air temperatures are shown for Surat and New Delhi. Surat's climate needs substantial cooling during the summer for 8 months (March–October) and the climate of New Delhi needs common cooling (April–October) months (mean temperature larger than or same as 29°C), additionally, both Surat and New Delhi require heating to maintain thermal comfort during winter months (December and January) due to an average atmospheric temperature less than 18°C.

In Surat, during the summer months (March–October), (April–June) have average environmental temperatures above 30°C. In New Delhi also average environmental temperature during these months (April–September) is over 30°C. For this reason, in the abovementioned summer months in Surat and New Delhi, latent heat absorption has been observed as 100%. So liquid fraction is 1 ( $\omega_1 = 1$ ). In Surat and New Delhi, the mean ambient temperature ( $\theta_a$ ) is lower than the typical freezing temperature ( $\theta_s$ ) during the winter period (December to January), and the 100% release of latent heat is possible, or a fraction of solid is 1 ( $\omega_s = 1$ ).

Equation (14) estimates yearly energy reductions ( $C_s$ ) as an outcome of decreasing cooling and heating loads.

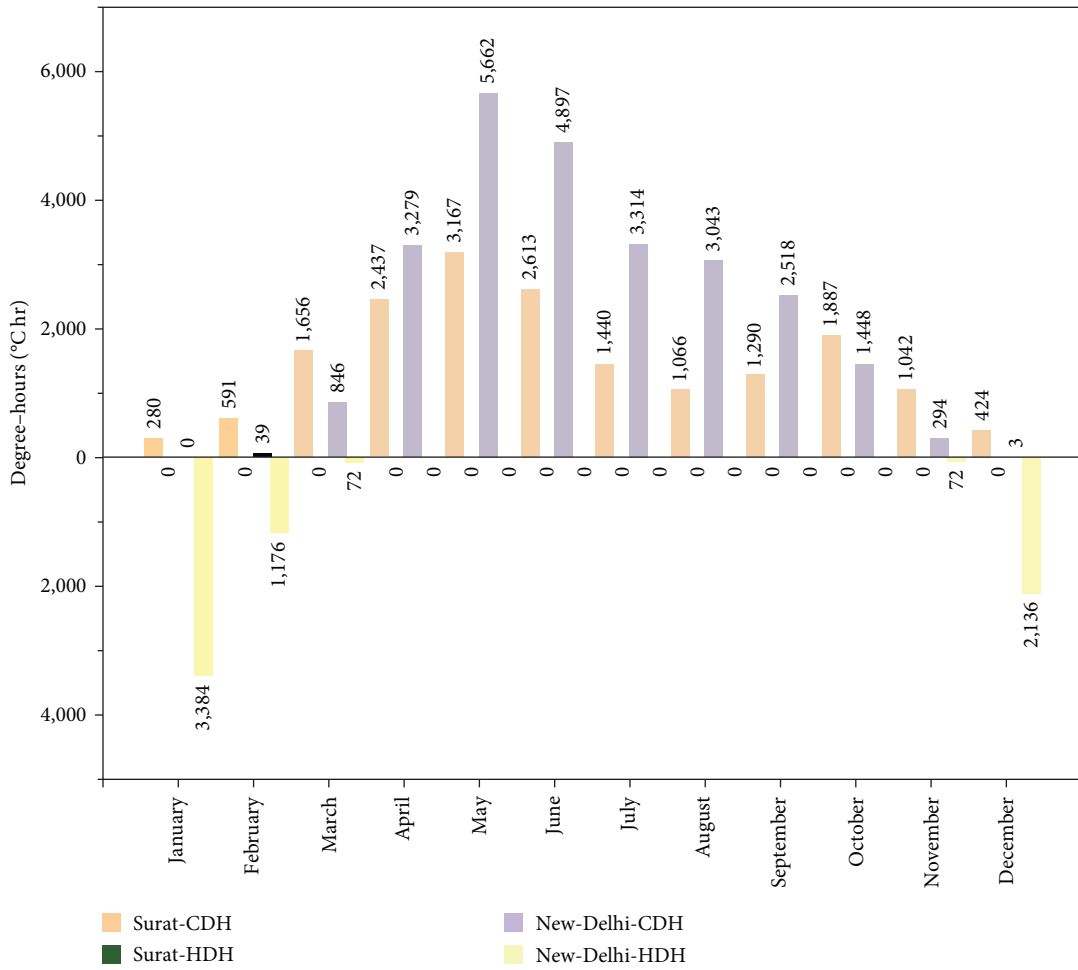


FIGURE 3: Cooling and heating degree-hours for Surat and New Delhi.

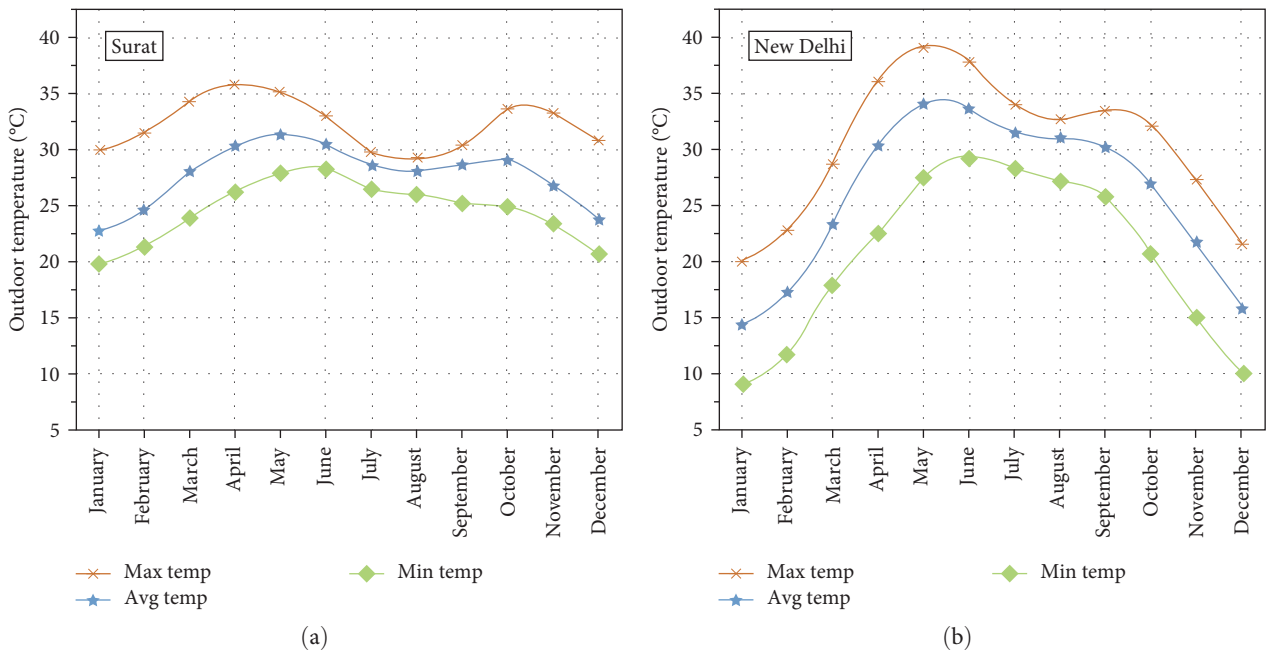


FIGURE 4: Monthly temperature (a) Surat and (b) New Delhi.



FIGURE 5: (a) Conventional roof building model; (b) PCM roof building model.

$$C_s = 10^{-3} \left[ C_{el} \frac{\left( u_{cy} \cdot CDH - \left( u_{pib}^l \cdot CDH - M \cdot L_{fg} \cdot 0.278 \cdot n_{cy} \right) \right)}{COP} + C_{ng} \frac{\left( u_{cy} \cdot HDH - \left( u_{pib}^s \cdot HDH - M \cdot L_{fg} \cdot 0.278 \cdot n_{cy} \right) \right)}{\eta} \right]. \quad (14)$$

According to Equation (14), the latent heat of PCM is denoted by  $L_{fg}$ , and  $M$  represents PCM's mass employed in the roof. PCM's cycles number goes through ( $n_{cy}$ ), throughout the summer period (Surat (244) and New Delhi (214)) and in the winter period (62). The unsteady transmittance of the conventional roof is denoted by  $u_{cy}$ , while unsteady transmittance of PCM's filled roof is denoted by  $u_{pib}$ . The unsteady transmittances ( $u_{pib}^s$  and  $u_{pib}^l$ ) of the winter and summer situations were calculated using the PCMs' solid and

liquid state thermal properties. Electricity and natural gas have cooling and heating prices ( $C_{el}$  and  $C_{ng}$ ) of 0.082 and 0.014 \$/kW hr, respectively. Similarly, the rate of (COP) coefficient of performance is 2.5 and the efficiency of natural gas power generation is 0.80, respectively [38]. When energy conservation measures are implemented, CO<sub>2</sub> emissions in the energy production plant are significantly decreased (Equation (15)).

$$m_{cer} = 10^{-3} \left[ m_a \frac{\left( u_{cy} \cdot CDH - \left( u_{pib}^l \cdot CDH - M \cdot L_{fg} \cdot 0.278 \cdot n_{cy} \right) \right)}{COP} + m_b \frac{\left( u_{cy} \cdot HDH - \left( u_{pib}^s \cdot HDH - M \cdot L_{fg} \cdot 0.278 \cdot n_{cy} \right) \right)}{\eta} \right]. \quad (15)$$

As shown in Equation (15), annual carbon mitigation owing to saving PCM's energy-filled roof is denoted by  $m_{cer}$ , and carbon mass discharge for electricity production (1.57 kg/kW hr) and natural gas production (0.18 kg/kW hr) are indicated by  $m_a$  and  $m_b$ , respectively [46].

Using Equation (16), payback duration (PT) calculates how long extensive it will take to recover increased capital expenditure related to PCMs ( $C_{PCM}$ ), after considering inflation ( $w = 7.6\%$ ) and interest charge ( $x = 6.6\%$ ).

$$PT = \frac{\ln \left[ \frac{C_{PCM} \cdot (w-x)}{C_s} + 1 \right]}{\ln \ln \frac{(1+w)}{(1+x)}}, \quad (16)$$

where PCM's capital outlay ( $C_{PCM}$ ) such as FS29, HS29, and OM29 are 5.05, 1.18, and 4.53 \$/kg, respectively [47].

**2.4. Justification of the Research Analysis.** For the goal of confirming the analytical conclusions, empirical data from two sequential building models constructed at VIT University and April month is evaluated. Coordinational information for VIT University is 12.91°N 79.13°E (South India). Figures 5(a) and 5(b) demonstrate the design of two similar building prototypes, one with and one without a PCM roof enclosure. Each model measures 0.5 m in width, 0.5 m in height, and 0.5 m in depth, and has a volume of 0.125 m<sup>3</sup>. Wall thickness is 0.0455 m for both the building models and the roof RCC thickness is 2.54 cm for the conventional roof and 2.54 cm (RCC) + 0.1 cm (GI casing thickness) + 0.8 cm (PCM thickness (OM30)) + 0.1 cm (GI casing thickness) for marcoencapsulated PCM roof envelope. Both building models were equipped with industry-calibrated heat flux detectors. Heat flux detectors have been utilized to evaluate entering heat

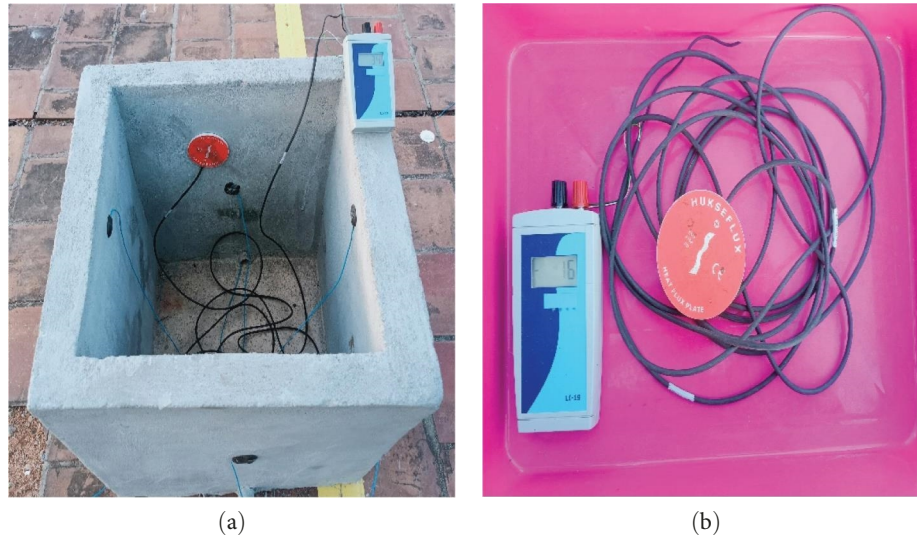


FIGURE 6: (a) Building model with heat flux sensor. (b) Heat flux sensor.

TABLE 5: Input variables for analytical research.

Input variables for analytical research	Values
The temperature of the surrounding environment on average during April ( $\theta_m$ )	28°C
Cooling degree-hours (CDH)	2,541°C hr
Liquid fraction ( $\omega_l$ )	0.6
PCM cycle number throughout April ( $n_{cy}$ )	30
Latent heat of PCM throughout April utilization ( $L_{fg}$ )	163.3 kJ/kg
Cyclic transmittance difference between prototype roof with and without PCM ( $u_{cy}$ )	1.13 W/m <sup>2</sup> K

flux from interior surfaces of structures in accordance with ASTM C1046, and data were collected for building types using an automated data recorder. The building model with a heat flux sensor is demonstrated in Figures 6(a) and 6(b), and suitable specifications are depicted in Table 5.

Figure 7(a) depicts the average heat flux (hourly) into the building prototypes with normal and PCM roof envelopes. During the daytime (6 a.m.–6 p.m.), the traditional building concept shows a considerable enhancement in heat flow into the building model when compared to the PCM roof envelope. The above case reverses during the nighttime. According to the experimental findings, during April, the traditional and PCM roof envelopes acquire 5.46 and 3.10 kW hr of heat, respectively. The PCM roof envelope building model achieves a practical heat gain decrease of 2.36 kW hr when compared to the traditional roof model. The input parameters for mathematical simulations are listed in Table 5.

In accordance with the mathematical simulation, the PCM roof envelope building model decreased heat intake by 2.74 kW hr when compared to the conventional roof building design. As shown in Figure 7(b), the experimental findings agree with the analytical results within a margin of 13.9% [48].

### 3. Results and Discussions

**3.1. Entire Air Conditioning Cost Abatement of RCC Roof Stuffed with Various PCMs.** To appraise the total air conditioning tariff abatement, a comparison between the RCC roof

integrated with PCM and the conventional roof is carried out using Equation (14). In Surat and New Delhi climates, Figure 8 demonstrates the total RCC roof's air conditioning cost savings filled with PCMs compared to a standard RCC roof. In the climate of Surat, FS29 PCM filled in various configurations (R-1, R-2, R-3, R-4, R-5, and R-6) results in total savings of \$3.40, \$3.33, \$3.33, \$3.37, \$3.34, and \$3.38 per meter square for air conditioning, respectively. FS29 PCM offers the greatest overall reduction in air conditioning costs of 3.40 \$/m<sup>2</sup> in R-1 roof configuration, among all other layouts in this group (R-1–R-6). RCC roof layout R1 filled with PCMs of FS29, HS29, and OM29 saves an overall air conditioning cost of 3.4, 6.29, and 3.98 \$/m<sup>2</sup>, respectively. In the R-1 roof arrangement, the HS29 PCM offers the greatest entire air conditioning cost reduction at \$6.29/m<sup>2</sup>, among all other layouts in this group (R-1–R-6). When all configurations are taken into account, FS29 has the lowest overall air conditioning cost savings compared to the other PCMs assessed.

Comparing several RCC roof designs stuffed with PCMs in New Delhi's climate, HS29 PCM in R-1 configuration exhibits the greatest overall cost savings in the air conditioning of \$6.61 per square meter. HS29 shows a better total air conditioning cost saving compared to other PCMs. R-2 and R-3 RCC roof configurations filled with FS29 show the least total air conditioning cost savings of 3.48 \$/m<sup>2</sup>.

Comparing the different RCC roof configurations in Surat and New Delhi climatic scenarios, the R-2 configuration stuffed

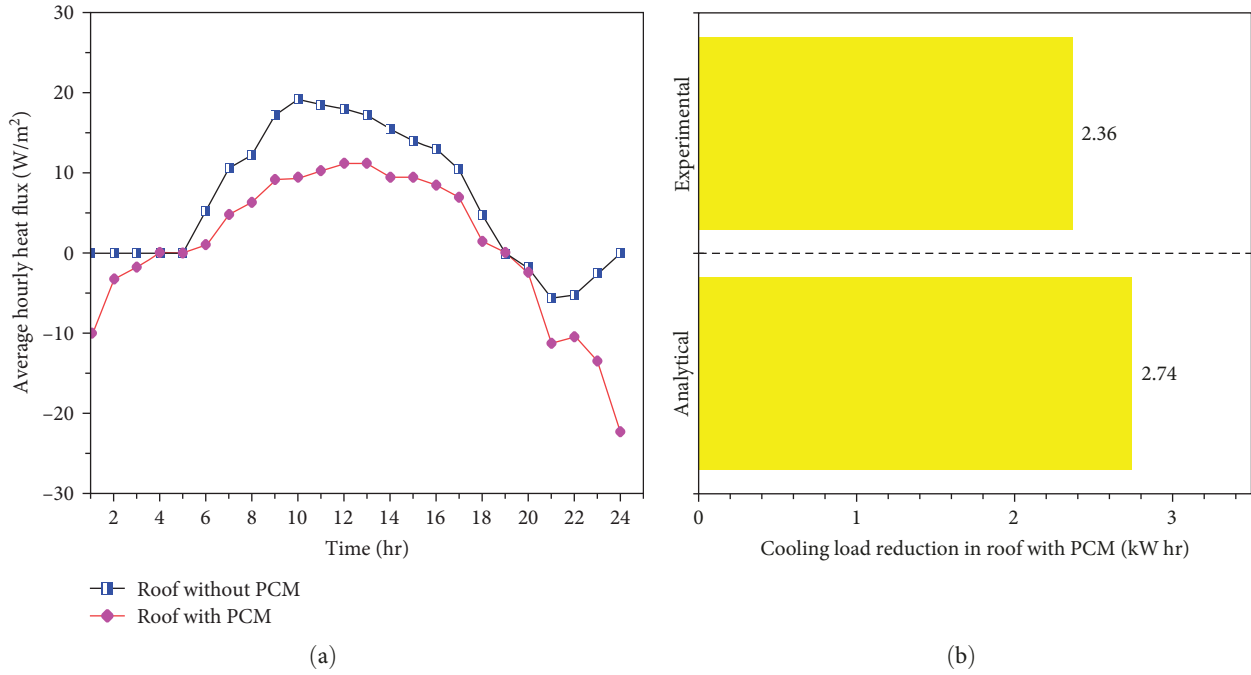


FIGURE 7: (a) Mean hourly heat intake in the prototype structures; (b) analytical and experimental evaluation of cooling load reductions in the roof with PCM.

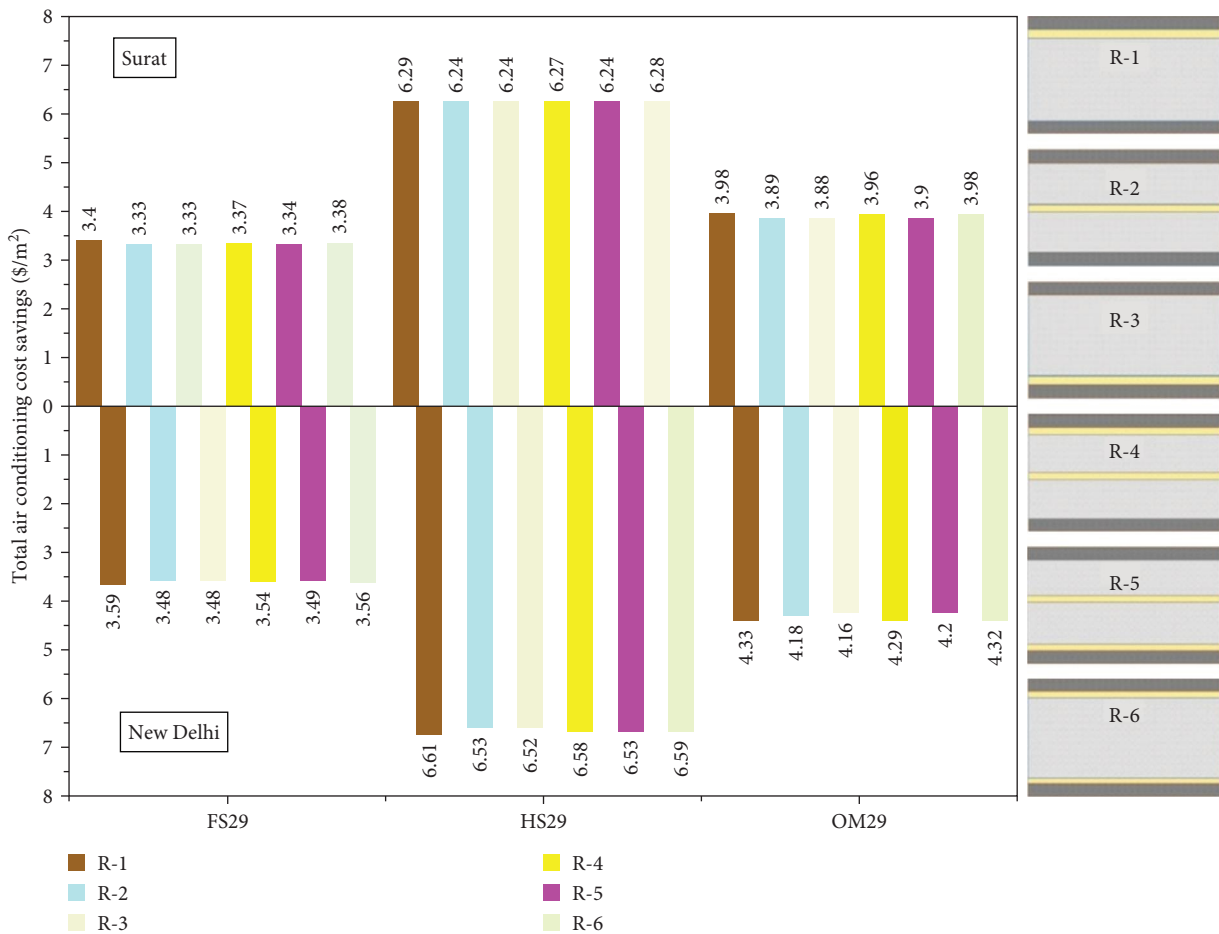


FIGURE 8: RCC roof's air conditioning cost savings stuffed with PCMs in Surat and New Delhi weather conditions.

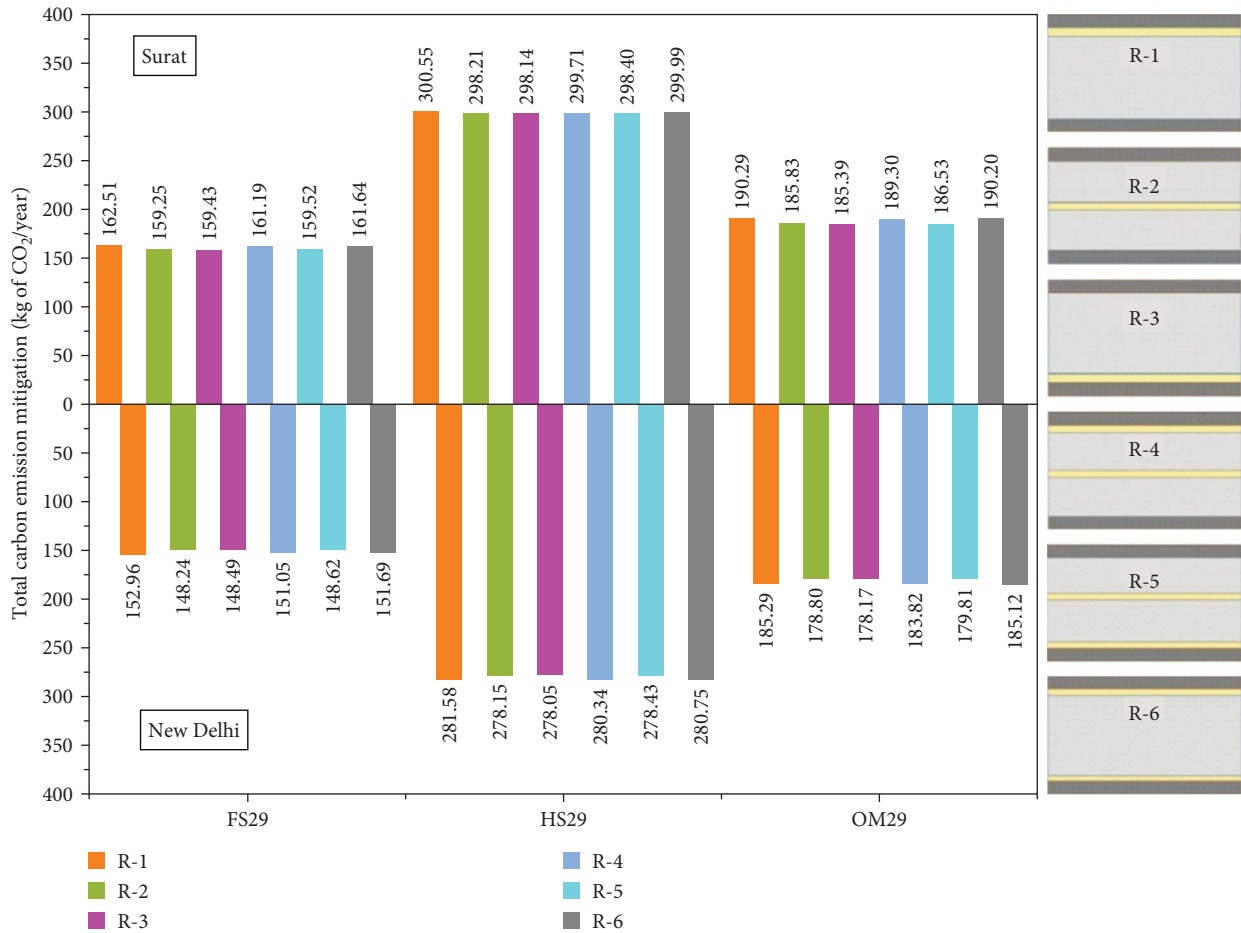


FIGURE 9: Carbon emission reduction of RCC roof stuffed with PCMs in Surat and New Delhi climates.

with HS29 shows a 46.8% increase in total air conditioning cost savings compared to the R-2 configuration stuffed with FS29. RCC roof configuration R-1 with OM29 results in an increase of 17% in the total cost of air conditioning compared to roof configuration R-1 with FS29. In the literature, it is reported that the time when the PCM begins to melt is delayed as the density of PCM increases, and the time range of liquid PCM reduces, indicating that the heat flows into the room decreases as the density of PCM increases [49]. The current study’s findings demonstrate that HS29 has a higher density, resulting in better thermal performance than FS29 and OM29.

**3.2. Carbon Exuding Reduction Prospective of RCC Roof Stuffed with Various PCMs.** The carbon emission reduction of the RCC roof stuffed with PCMs and standard RCC roof is obtained using Equation (15). In Surat and New Delhi weather conditions, the carbon-exuding reduction prospective of the RCC roof stuffed with PCMs is demonstrated in Figure 9.

In Surat, FS29 PCM filled in different layouts (R-1, R-2, R-3, R-4, R-5, and R-6) exhibits a total carbon emission reduction of 162.51, 159.25, 159.43, 161.19, 159.52, 161.64 kg of CO<sub>2</sub>/year, respectively. FS29 PCM exhibits maximum total carbon emission degradation of 162.51 kg of CO<sub>2</sub>/year in the R-1 roof configuration, among all other layouts in this group (R-1–R-6). RCC roof configuration R-1 integrated with PCMs

FS29, HS29, and OM29 exhibits a total carbon emission reduction of 162.51, 300.55, and 190.29 kg of CO<sub>2</sub>/year, respectively. HS29 PCM in the R-1 roof layout demonstrated the greatest carbon emission reduction compared to all other PCMs in the same layout; a total carbon emission mitigation of 300.55 kg of CO<sub>2</sub>/year was achieved as a result of significant savings in air conditioning costs. After investigating different configurations of (R-1–R-6), the R-1 configuration shows the highest carbon emission mitigation among all other configurations. FS29 in R-2 configuration showed the least sum carbon emission mitigation of 159.25 kg of CO<sub>2</sub>/year.

In New Delhi, the R-1 configuration filled with HS29 maximum sum carbon emission mitigation of 281.58 kg of CO<sub>2</sub>/year. RCC roof configuration R-1 filled with HS29 demonstrates an increment of 84% in carbon emission reduction compared to RCC roof configuration R-1 with FS29.

**3.3. Payback Durations of RCC Roof Stuffed with PCMs.** The payback span of the RCC roof filled with PCMs was evaluated by using Equation (16). In Surat and New Delhi climates, the payback span in years of RCC roofs filled with PCMs is demonstrated in Figure 10.

In Surat, FS29 PCM filled in different layouts (R-1, R-2, R-3, R-4, R-5, and R-6) shows the payback periods of 14.68, 14.96, 14.95, 14.80, 14.94, and 14.76 years, respectively. FS29

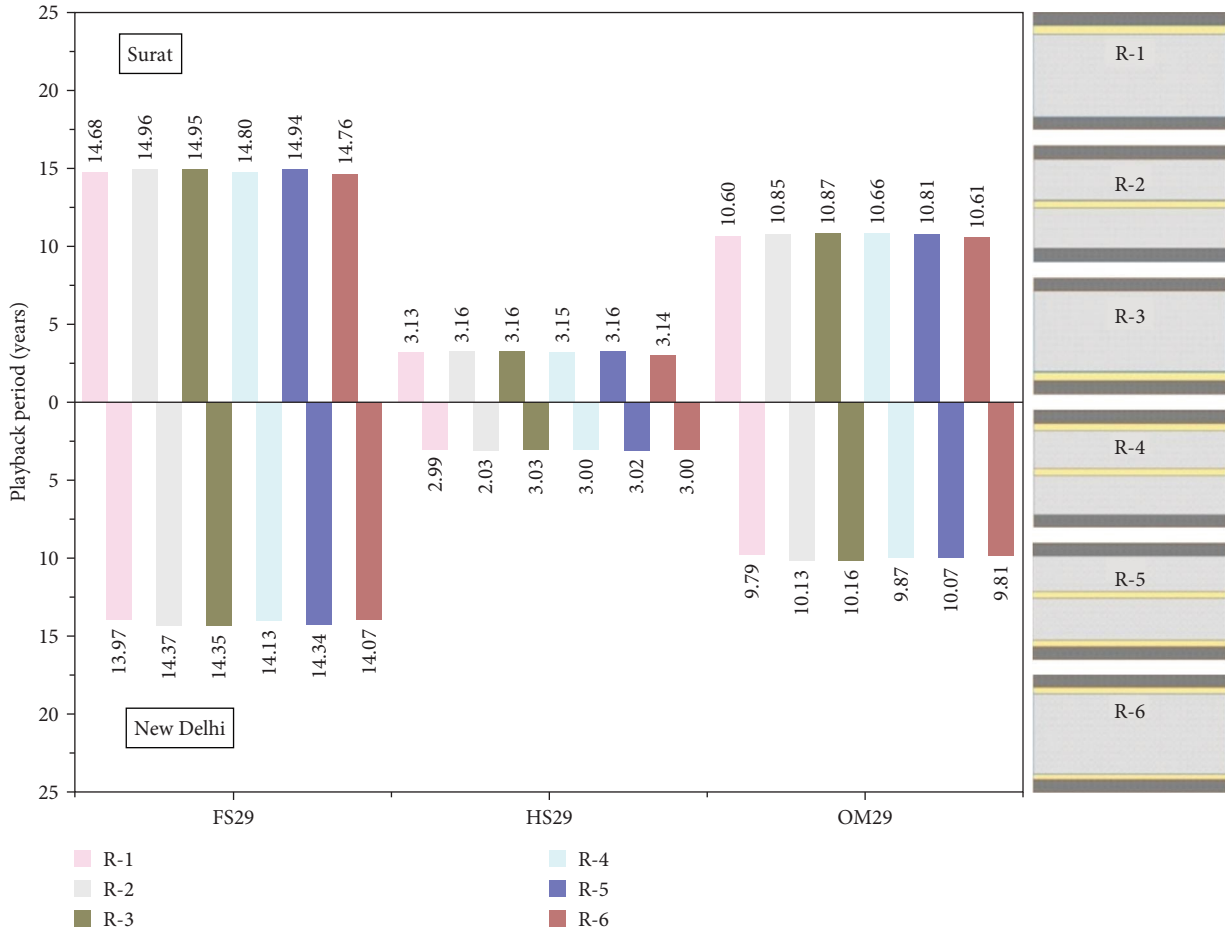


FIGURE 10: Payback duration of RCC roof stuffed with PCMs in Surat and New Delhi climates.

PCM shows the payback periods of 14.68 years in the R-1 roof configuration, among all other layouts in this group (R-1–R-6). RCC roof configuration R-1 filled with FS29, HS29, and OM29 PCMs have payback periods of 14.68, 3.13, and 10.60 years, respectively. By investigating all PCMs in various layouts, HS29 shows the least payback duration of 3.13 years, and FS29 results in the highest payback duration of 14.96 years. According to an economic analysis of all three of the PCMs, the HS29 PCM is the most cost-effective than FS29 and OM29.

HS29, OM29, and FS29 are the sequential order of PCMs for a low payback period. Layouts R-1, R-6, R-4, R-5, R-2, and R-3 are in a sequence with a low to high payback timeframe. The most important aspect in calculating the payback duration for PCM-filled roofs is the price and optimum placement of the material.

The PCM position, unsteady transmittance, and latent heat of PCM’s fusion are the most influential criteria for higher air conditioning cost savings of roofs. The unsteady or periodic thermal transmittance of the HS29 PCM integrated roof is lower (dependent on TC, specific heat, and density) and the fusion’s latent heat is higher. Because of the aforementioned factors, HS29 PCM-integrated roofs outperform other PCM-integrated roofs in terms of thermoeconomic performance. The lowest payback period of HS29 is

due to the lowest capital cost and highest air conditioning cost savings of HS29 when compared to organic mixtures and form stable mixtures. The abovementioned study findings are applicable to hot–arid and warm-temperate climatic situations, respectively.

Extended surfaces (fins) are of vital importance in the charging and discharging processes of PCM-reinforced building roofs. Using improved fin shapes in such systems is helpful for increased heat dissipation and higher thermal performance values. Perturbation-based numerical techniques can be utilized in further works to optimize fin profiles, heat dissipation rates, fin efficiency, and fin effectiveness [50–52]. Heat transfer enhancement can also be further improved by perforations [53, 54]. Due to the poor TC of PCMs, it is recommended to consider PCM roofs with the said optimized extended surfaces.

#### 4. Conclusions

Thermophysical properties of RCC and different PCMs were measured experimentally as part of this study. Experimental investigations were performed in Vellore’s weather scenarios to authenticate theoretical results. Thermoeconomic analyses of several PCM-stuffed roof configurations were performed to determine the optimal roof design, energy-efficient PCMs,

and ecologically friendly components under two distinct climatic conditions.

- (i) When considering all six roof layouts (R-1–R-6) and three PCMs (FS29, HS29, and OM29), roof layout R-1 filled with HS29 reduces 6.29 and 6.61  $\$/m^2$  for Surat and New Delhi, respectively, in total air conditioning pricing.
- (ii) Among the three PCMs (FS29, HS29, and OM29) with six layouts (R-1–R-6) studied in India's hot–arid and warm-temperate climates, the R-1 configuration filled with HS29 minimizes the most carbon emissions, 300.55 and 281.58 kg  $CO_2$ /year, respectively.
- (iii) R-1 with HS29 had the lowest payback time of 3.13 years of all the roof layouts (R-1–R-6) with different PCMs (FS29, HS29, and OM29). R-1, R-6, R-4, R-5, R-2, and R-3 are the selection order for low payback span roof layouts. The PCM's choice of order for a shorter refund period is appropriate in both hot–arid and warm-temperate zones are HS29, OM29, and FS29.

The hydrated salt HS29 PCM ensures the best overall energy cost reductions, the biggest drop in carbon emission, and the quickest refund time-frames for use in the hot-parched and warm-temperate regions of India. In the following sequence, R-1 > R-6 > R-4 > R-5 > R-2 > R-3 are the roof configurations that give the most cost-effectual air conditioning, the highest decrease in carbon emissions, and the fastest refund time. The PCM layer placed above the RCC (R-1, outer) gives better results because the PCM layer in the R-1 position will store most of the heat coming into the building and stop the heat from moving to the inside roof surface. The performance in the building was maximized by PCMs situated either on the building's exterior or in close proximity to its heat sources, as these PCMs required less effort to charge and discharge. Due to its superior properties, including its high latent heat and density, the HS29 PCM provides the greatest savings in air conditioning costs.

The findings of this research will be relevant to the development of energy-efficient building envelopes with PCMs for green energy buildings. Future research might focus on energy-efficient facades merged with various novel PCMs in diverse combinations.

## Nomenclature

B:	Cyclic thickness (–)
$C_{el}$ :	Electricity cost for cooling ( $\$/kW$ hr)
$C_{ng}$ :	Heating cost due to natural gas ( $\$/kW$ hr)
$C_p$ :	Specific heat (J/kg K)
$C_{PCM}$ :	Capital expenditure of PCM ( $\$/kg$ )
$C_s$ :	Annual energy cost saving ( $\$/m^2$ )
D:	Characteristic admittance of slab (–)
H:	PCM's latent heat of (kJ/kg)
$Hf_1$ :	Incoming heat flux to the roof interior ( $W/m^2$ )
H:	Heat transfer coefficient ( $W/m^2K$ )
k:	Thermal conductivity

$L_{fg}$ :	PCM's latent heat for utilization (kJ/kg)
M:	PCM's mass for utilization (kg)
$m_a$ and $m_b$ :	Mass of carbon emission (kg of $CO_2/kW$ hr)
$m_{cer}$ :	Mass of carbon emission reduction (kg/year)
$n_{cy}$ :	Number of PCM cycles
P:	Cyclic period (s)
Q:	Cyclic heat flux ( $W/m^2$ )
$Tr_1$ :	Thermal resistivity for heat flow ( $m^2 K/W$ )
$u_{cyc}$ :	Cyclic transmittance ( $W/m^2K$ )
W:	Inflation rate (%)
X:	Interest rate (%)
Y:	Building material thickness (m).

## Subscript

In:	Inside
Ou:	Outside.

## Superscript

L:	Liquid
S:	Solid.

## Greek Letters

$\delta$ :	Thermal conductivity ( $W/mK$ )
$\eta$ :	Natural gas power generation efficiency
$\theta$ :	Cyclic temperature ( $^{\circ}C$ )
$\theta_L$ :	PCM melting temperature ( $^{\circ}C$ )
$\theta_a$ :	Mean ambient temperature ( $^{\circ}C$ )
$\theta_{max}$ :	Maximum outdoor air temperature ( $^{\circ}C$ )
$\theta_{min}$ :	Minimum outdoor air temperature ( $^{\circ}C$ )
$\theta_p$ :	Phase change temperature ( $^{\circ}C$ )
$\theta_r$ :	Reference temperature ( $^{\circ}C$ )
$\theta_s$ :	PCM freezing temperature ( $^{\circ}C$ )
$\rho$ :	Density ( $kg/m^3$ )
$\omega_{l/s}$ :	Liquid/solid fraction.

## Acronyms

CDH:	Degree–hours for cooling
COP:	Coefficient of performance
DSC:	Differential scanning calorimetry
FS29:	Form stable mixture-29
HDH:	Degree–hours for heating
HS29:	Hydrated salt-29
OM29:	Organic mixture-29
OM30:	Organic mixture-30
PCM:	Phase change materials
PT:	Payback time
RCC:	Reinforced cement concrete.

## Data Availability

No underlying data were collected or produced in this study.

## Conflicts of Interest

The authors declare that they have no conflicts of interest.

## References

- [1] J. Zhao and S. Li, "Life cycle cost assessment and multi-criteria decision analysis of environment-friendly building insulation materials—a review," *Energy and Buildings*, vol. 254, Article ID 111582, 2022.
- [2] P. Nejat, F. Jomehzadeh, M. M. Taheri, M. Gohari, and M. Z. A. Majid, "A global review of energy consumption, CO<sub>2</sub> emissions and policy in the residential sector (with an overview of the top ten CO<sub>2</sub> emitting countries)," *Renewable and Sustainable Energy Reviews*, vol. 43, pp. 843–862, 2015.
- [3] M. Mathur, *Energy Benchmarks for Commercial Buildings*, Bureau of Energy Efficiency, Sewa Bhawan, R.K. Puram, New Delhi, 2021.
- [4] H. Akeiber, P. Nejat, M. Z. A. Majid et al., "A review on phase change material (PCM) for sustainable passive cooling in building envelopes," *Renewable and Sustainable Energy Reviews*, vol. 60, pp. 1470–1497, 2016.
- [5] S. D. Attri, A. Tyagi, and Climate Profile of India, *Environment Monitoring and Research Center*, pp. 1–129, India Meteorology Department, New Delhi, India, 2010.
- [6] X. Zhu, W. Feng, J. Song, Y. Niu, L. Yang, and J. Liu, "Impact of orientation, position, thermal insulation layer and seasonal variation on thermal storage performance of walls: a one-year-round field-test study," Position, Thermal Insulation Layer and Seasonal Variation on Thermal Storage Performance of Walls: A One-Year-Round Field-Test Study
- [7] J. S. Sage-Lauck and D. J. Sailor, "Evaluation of phase change materials for improving thermal comfort in a super-insulated residential building," *Energy and Buildings*, vol. 79, pp. 32–40, 2014.
- [8] A. Pasupathy, R. Velraj, and R. V. Seeniraj, "Phase change material-based building architecture for thermal management in residential and commercial establishments," *Renewable and Sustainable Energy Reviews*, vol. 12, no. 1, pp. 39–64, 2008.
- [9] D. Mazzeo, N. Matera, N. Arcuri, and F. Barreca, "A multilayer panel in cork and natural phase change materials: thermal and energy analysis," *E3S Web of Conferences*, vol. 312, Article ID 02003, 2021.
- [10] C. K. Halford and R. F. Boehm, "Modeling of phase change material peak load shifting," *Energy and Buildings*, vol. 39, no. 3, pp. 298–305, 2007.
- [11] N. Matera, P. Bevilacqua, N. Arcuri, G. Oliveti, D. Mazzeo, and P. Romagnoni, "Optimal design of PCM in internal walls for nZEB buildings," in *2018 IEEE International Conference on Environment and Electrical Engineering and 2018 IEEE Industrial and Commercial Power Systems Europe (EEEIC/I&CPS Europe)*, pp. 1–6, IEEE, Palermo, Italy, 2018.
- [12] D. Mazzeo and G. Oliveti, "Parametric study and approximation of the exact analytical solution of the Stefan problem in a finite PCM layer in a steady periodic regime," *International Communications in Heat and Mass Transfer*, vol. 84, pp. 49–65, 2017.
- [13] E. Osterman, V. Butala, and U. Stritih, "PCM thermal storage system for 'free' heating and cooling of buildings," *Energy and Buildings*, vol. 106, pp. 125–133, 2015.
- [14] S. Mondal, "Phase change materials for smart textiles—an overview," *Applied Thermal Engineering*, vol. 28, no. 11-12, pp. 1536–1550, 2008.
- [15] D. Li, Y. Wu, C. Liu, G. Zhang, and M. Arıcı, "Energy investigation of glazed windows containing Nano-PCM in different seasons," *Energy Conversion and Management*, vol. 172, pp. 119–128, 2018.
- [16] L. Navarro, A. Solé, M. Martín et al., "Benchmarking of useful phase change materials for a building application," *Energy and Buildings*, vol. 182, pp. 45–50, 2019.
- [17] H. Mehling and L. F. Cabeza, "Solid-liquid phase change materials," in *Heat and Cold Storage with PCM*, Heat and Mass Transfer, pp. 11–55, Springer, Berlin, Heidelberg, 2008.
- [18] X. Sun, K. O. Lee, M. A. Medina, Y. Chu, and C. Li, "Melting temperature and enthalpy variations of phase change materials (PCMs): a differential scanning calorimetry (DSC) analysis," *Phase Transitions*, vol. 91, no. 6, pp. 667–680, 2018.
- [19] S. S. Chandel and T. Agarwal, "Review of current state of research on energy storage, toxicity, health hazards and commercialization of phase changing materials," *Renewable and Sustainable Energy Reviews*, vol. 67, pp. 581–596, 2017.
- [20] P. K. S. Rathore and S. K. Shukla, "Potential of macro-encapsulated PCM for thermal energy storage in buildings: a comprehensive review," *Construction and Building Materials*, vol. 225, pp. 723–744, 2019.
- [21] G. Gholamibozanjani and M. Farid, "A critical review on the control strategies applied to PCM-enhanced buildings," *Energies*, vol. 14, no. 7, Article ID 1929, 2021.
- [22] S. Alvarez, L. F. Cabeza, A. Ruiz-Pardo, A. Castell, and J. A. Tenorio, "Building integration of PCM for natural cooling of buildings," *Applied Energy*, vol. 109, pp. 514–522, 2013.
- [23] A. Tokuç, T. Başaran, and S. C. Yesügey, "An experimental and numerical investigation on the use of phase change materials in building elements: the case of a flat roof in Istanbul," *Energy and Buildings*, vol. 102, pp. 91–104, 2015.
- [24] A. Pasupathy and R. Velraj, "Effect of double layer phase change material in building roof for year round thermal management," *Energy and Buildings*, vol. 40, no. 3, pp. 193–203, 2008.
- [25] A. Chelliah, S. Saboor, A. Ghosh, and K. J. Kontoleon, "Thermal behaviour analysis and cost-saving opportunities of PCM-integrated terracotta brick buildings," *Advances in Civil Engineering*, vol. 2021, Article ID 6670930, 15 pages, 2021.
- [26] S. J. Chang, S. Wi, S.-G. Jeong, and S. Kim, "Thermal performance evaluation of macro-packed phase change materials (PCMs) using heat transfer analysis device," *Energy and Buildings*, vol. 117, pp. 120–127, 2016.
- [27] Y. H. Zhang, *Preparation of the PCM Roof Brick and Study on Its Thermal Insulation Properties*, M.S. Thesis, Scientific Dissertation of Guangzhou University, 2012.
- [28] I. Baskar and M. Chellapandian, "Experimental and finite element analysis on the developed real-time form stable PCM based roof system for thermal energy storage applications," *Energy and Buildings*, vol. 276, Article ID 112514, 2022.
- [29] M. Thambidurai, K. Panchabikesan, K. M. N., and V. Ramalingam, "Review on phase change material based free cooling of buildings—the way toward sustainability," *Journal of Energy Storage*, vol. 4, pp. 74–88, 2015.
- [30] X. Mi, R. Liu, H. Cui, S. A. Memon, F. Xing, and Y. Lo, "Energy and economic analysis of building integrated with PCM in different cities of China," *Applied Energy*, vol. 175, pp. 324–336, 2016.
- [31] H. J. Alqallaf and E. M. Alawadhi, "Concrete roof with cylindrical holes containing PCM to reduce the heat gain," *Energy and Buildings*, vol. 61, pp. 73–80, 2013.

- [32] IS 10262, "2019 Concrete Mix Proportioning—Guidelines," Bureau of Indian Standard, New Delhi, 2019.
- [33] M. M. Kenisarin and K. M. Kenisarina, "Form-stable phase change materials for thermal energy storage," *Renewable and Sustainable Energy Reviews*, vol. 16, no. 4, pp. 1999–2040, 2012.
- [34] ASTM D5334-14, "Standard test method for determination of thermal conductivity soil and soft rock by thermal needle probe procedure," vol. 4, pp. 6–13, 2011.
- [35] C. Arumugam and S. Shaik, "Air-conditioning cost saving and CO<sub>2</sub> emission reduction prospective of buildings designed with PCM integrated blocks and roofs," *Sustainable Energy Technologies and Assessments*, vol. 48, Article ID 101657, 2021.
- [36] J. P. Holman, *Experimental Methods for Engineers*, McGraw-Hill Companies, 2012.
- [37] M. Davies, *Building Heat Transfer*, John Wiley & Sons Ltd, 2004.
- [38] C. Arumugam and S. Shaik, "Transforming waste disposals into building materials to investigate energy savings and carbon emission mitigation potential," *Environmental Science and Pollution Research*, vol. 28, no. 12, pp. 15259–15273, 2021.
- [39] G. M. Soret, P. Vacca, J. Tignard et al., "Thermal inertia as an integrative parameter for building performance," *Journal of Building Engineering*, vol. 33, Article ID 101623, 2021.
- [40] A. Guide, *Environmental Design*, Chartered Institute of Building Services Engineers (CIBSE), 2006.
- [41] S. Shaik and A. B. T. P. Setty, "Influence of ambient air relative humidity and temperature on thermal properties and unsteady thermal response characteristics of laterite wall houses," *Building and Environmental*, vol. 99, pp. 170–183, 2016.
- [42] ASHRAE, "Climatic design information," in *ASHRAE Fundamentals Handbook*, ASHRAE, 2009.
- [43] M. Arıcı, F. Bilgin, S. Nižetić, and H. Karabay, "PCM integrated to external building walls: an optimization study on maximum activation of latent heat," *Applied Thermal Engineering*, vol. 165, Article ID 114560, 2020.
- [44] S. Shaik, C. Arumugam, S. V. Shaik, M. Arıcı, A. Afzal, and Z. Ma, "Strategic design of PCM integrated burnt clay bricks: potential for cost-cutting measures for air conditioning and carbon dioxide extenuation," *Journal of Cleaner Production*, vol. 375, Article ID 134077, 2022.
- [45] A. Mani and S. Rangarajan, *Solar Radiation Hand Book*, pp. 1986–2000, Allied Publishers Private Limited, India, 1982.
- [46] A. Chel and G. N. Tiwari, "Performance evaluation and life cycle cost analysis of earth to air heat exchanger integrated with adobe building for New Delhi composite climate," *Energy and Buildings*, vol. 41, no. 1, pp. 56–66, 2009.
- [47] J. A. Duffie and W. A. Beckman, *Solar Engineerng of Thermal Processes*, Solar Energy Laboratory University of Wisconsin-Madson, 2013.
- [48] S. Kalaiselvam, R. Parameshwaran, and S. Harikrishnan, "Analytical and experimental investigations of nanoparticles embedded phase change materials for cooling application in modern buildings," *Renewable Energy*, vol. 39, no. 1, pp. 375–387, 2012.
- [49] D. Li, Z. Li, Y. Zheng, C. Liu, A. K. Hussein, and X. Liu, "Thermal performance of a PCM-filled double-glazing unit with different thermophysical parameters of PCM," *Solar Energy*, vol. 133, pp. 207–220, 2016.
- [50] E. Cuce and P. M. Cuce, "Homotopy perturbation method for temperature distribution, fin efficiency and fin effectiveness of convective straight fins with temperature-dependent thermal conductivity," *Proceedings of the Institution of Mechanical Engineers, Part C: Journal of Mechanical Engineering Science*, vol. 227, no. 8, pp. 1754–1760, 2013.
- [51] P. M. Cuce, E. Cuce, and C. Aygun, "Homotopy perturbation method for temperature distribution, fin efficiency and fin effectiveness of convective straight fins," *International Journal of Low-Carbon Technologies*, vol. 9, no. 1, pp. 80–84, 2014.
- [52] E. Cuce and P. M. Cuce, "A successful application of homotopy perturbation method for efficiency and effectiveness assessment of longitudinal porous fins," *Energy Conversion and Management*, vol. 93, pp. 92–99, 2015.
- [53] E. Cuce, E. K. Oztekin, and P. M. Cuce, "Heat transfer enhancement in cylindrical fins through longitudinal parabolic perforations," *International Journal of Ambient Energy*, vol. 40, no. 4, pp. 406–412, 2019.
- [54] E. Cuce, "Boyuna uzatılmış yüzeylerde dikdörtgensel oyukların ısı atımına etkisi: bir hesaplamalı akışkanlar dinamiği analizi," *Afyon Kocatepe Üniversitesi Fen ve Mühendislik Bilimleri Dergisi*, vol. 20, no. 5, pp. 931–940, 2020.